



# 1 A coupled stochastic rainfall-evapotranspiration model 2 for hydrological impact analysis

3 Minh Tu Pham\*<sup>1</sup>, Hilde Vernieuwe<sup>2</sup>, Bernard De Baets<sup>2</sup>, and Niko E. C. Verhoest<sup>1</sup>

4 <sup>1</sup>Laboratory of Hydrology and Water Management, Ghent University, Coupure  
5 links 653, 9000 Ghent, Belgium

6 <sup>2</sup>KERMIT, Department of Mathematical Modelling, Statistics and Bioinformatics,  
7 Ghent University, Coupure links 653, 9000 Ghent, Belgium

8

## 9 Abstract

10 A hydrological impact analysis concerns the study of the consequences of certain scenarios  
11 on one or more variables or fluxes in the hydrological cycle. In such exercise, discharge is often  
12 considered, as especially extreme high discharges often cause damage due to the coinciding  
13 floods. Investigating extreme discharges generally requires long time series of precipitation and  
14 evapotranspiration that are used to force a rainfall-runoff model. However, such kind of data  
15 may not be available and one should resort to stochastically-generated time series, even though  
16 the impact of using such data on the overall discharge, and especially on the extreme discharge  
17 events is not well studied. In this paper, stochastically-generated rainfall and coinciding  
18 evapotranspiration time series are used to force a simple conceptual hydrological model. The  
19 results obtained are comparable to the modelled discharge using observed forcing data. Yet,  
20 uncertainties in the modelled discharge increase with an increasing number of stochastically-  
21 generated time series used. Notwithstanding this finding, it can be concluded that using  
22 a coupled stochastic rainfall-evapotranspiration model has a large potential for hydrological  
23 impact analysis.

## 24 1 Introduction

25 Precipitation is the most important variable in the terrestrial hydrological cycle that determines  
26 soil moisture and discharge from a watershed. As such, it also impacts water management where  
27 generally the occurrences of extreme events, e.g. storms or droughts, which have very low frequen-  
28 cies, are of concern. Very long time series of precipitation are hence needed. Because this kind of  
29 data is not always available, one may consider using a stochastically-generated rainfall time series  
30 (Boughton and Droop, 2003). Stochastic rainfall models can be used to produce very long time  
31 series or to compensate for missing data from finite historical records (Wilks and Wilby, 1999).  
32 Several types of rainfall models have been proposed in literature. Onof et al. (2000) grouped all  
33 continuous rainfall models into four types: (1) meteorological models; (2) stochastic multi-scale  
34 models; (3) statistical models and (4) stochastic process models. Meteorological models are capa-  
35 ble to describe the physical processes of all weather variables, including rainfall, by making use of  
36 very large and complex sets of equations. Numerical Weather Prediction and General Circulation  
37 Models are two common examples of this type of models. Stochastic multi-scale models describe  
38 the spatial evolution of the rainfall process regardless of scale factors. In general, these models  
39 involve an assumption of temporal invariance of rainfall over a range of scales (Bernardara et al.,  
40 2007). Statistical models, which can be used for simulating the precipitation trends, usually treat

\*MinhTu.Pham@UGent.be



41 the occurrence and the amount of precipitation separately (Wilks and Wilby, 1999). The rain-  
42 fall occurrence is represented by a sequence of dry and wet periods, usually simulated by Markov  
43 chains or Alternating Renewal Models. The precipitation amounts can be arbitrarily generated by  
44 making use of some popular distributions, e.g. the exponential (Todorovic and Woolhiser, 1975),  
45 the Gamma (Stern and Coe, 1984; Viglione et al., 2012) or the mixed exponential distribution  
46 (Woolhiser and Roldán, 1982; Wilks, 1998; Mason, 2004). Stochastic process models use simple  
47 assumptions of physical processes to simulate the hierarchical structure of the rainfall process.  
48 In this approach, only a limited number of parameters is needed (Verhoest et al., 2010). The  
49 Bartlett-Lewis (BL) (Rodríguez-Iturbe et al., 1987a) and the Neyman-Scott (Kavvas and Delleur,  
50 1981) models are the most commonly used models of this type. In this study, we only focus on  
51 the BL models. These models have been applied successfully in different areas, such as Great  
52 Britain (Onof and Wheat, 1993; Onof et al., 1994; Cameron et al., 2000), Ireland (Khaliq and  
53 Cunnane, 1996), Belgium (Verhoest et al., 1997; Vandenberghe et al., 2010; Vanhaute et al., 2012),  
54 the United States of America (Rodríguez-Iturbe et al., 1987b; Velghe et al., 1994), New Zealand  
55 (Cowpertwait et al., 2007), Australia (Gyasi-Agyei, 1999; Heneker et al., 2001) and South-Africa  
56 (Smithers et al., 2002). The BL models are chosen in this study for three main reasons: (1) they  
57 show a good performance in all recent studies; (2) they are capable of generating time series at a  
58 sufficient fine time scale (less than 1 hour); (3) their calibration is easy given the limited number  
59 of parameters; and (4) they mimic well the stochastic behavior of the historical time series at  
60 Uccle (Verhoest et al., 1997; Vanhaute et al., 2012), which is used in this study.

61  
62 Besides precipitation, the water balance is also highly influenced by the amount of water that  
63 is lost due to evapotranspiration. An accurate estimation of evapotranspiration is very essential  
64 for hydrological and agricultural designs, irrigation plans and for water distribution management  
65 (Droogers and Allen, 2002). The daily reference evapotranspiration is often modelled based on the  
66 Penman, Priestley–Taylor or Hargraeves equations; however, one major limitation of these models  
67 is that they require extensive input data, such as daily mean temperature, wind speed, relative  
68 humidity and solar radiation, which are not always available. Therefore, one may consider to rely  
69 on another approach based on stochastically-generated time series. More importantly, in order to  
70 obtain a correct evaluation of the water balance of a catchment and its discharge, these stochastic  
71 evapotranspiration data need to be consistent with the accompanying precipitation time series  
72 data (Pham et al., 2016). In this case, we can make use of the copula-based approach introduced  
73 in the work of Pham et al. (2016) in which the statistical dependence between evapotranspiration,  
74 precipitation and temperature is described by three- and four-dimensional vine copulas.

75  
76 Many modelling approaches exist for simulating catchment discharge. The simplest models are  
77 the conceptual models in which several (non-)linear reservoirs are put in series and/or parallel.  
78 Well-known examples of such conceptual models are: the Hydrologiska Byråns Vattenbalansavdel-  
79 ning model (Bergström, 1995), the NedborAfstromnings Model (Nielsen and Hansen, 1973) and  
80 the Probability Distributed Model (PDM) (Moore, 2007). Alternatively, physically-based models  
81 are based on scientific knowledge of different hydrological processes and their interactions. Gener-  
82 ally, these models contain many more parameters than the conceptual ones and require more input  
83 data, such as soil type, vegetation-related information, etc. Well-known examples of such models  
84 are the Soil and Water Assessment Tool (Arnold et al., 1998), the Système Hydrologique Européen  
85 (Abbott et al., 1986) and the Common Land Model (Dai et al., 2003). In this study, we do not  
86 intend to seek for the best hydrological model to assess our objective, but we opt for a model that  
87 is used in operational water management. More specifically, we will use PDM, as this model is  
88 used by the Flemish Environmental Agency (Cabus, 2008), and apply it to a catchment in Flan-  
89 ders, Belgium. The objective of this research is to assess whether the BL stochastically-generated  
90 rainfall and consistent evapotranspiration time series can be used for hydrological impact analyses.  
91 More specifically, we will evaluate different ways to apply stochastically modelled time series as  
92 forcing data to simulate the catchment's discharge. By increasing the number of stochastically-  
93 generated inputs to the model, we will assess the increase of uncertainty in modelled extremes  
94 and what portion of this increase can be attributed to the different stochastic generators. Sec-  
95 tion 3 first briefly introduces the coupled stochastic rainfall-evapotranspiration model and all the  
96 considered situations to simulate discharge from stochastic forcing data. Section 2 describes the

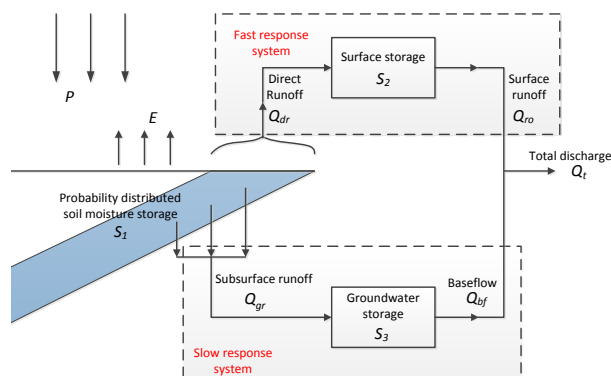


Figure 1: General model structure of the PDM (adapted from Moore, 2007).

97 historical records and all models used within this study. The discharge simulations from different  
 98 scenarios are then evaluated in Section 4 allowing for assessing the impact of stochastic data on  
 99 the simulation of discharge. Finally, conclusions and recommendations are given in Section 5.

## 100 2 Data and models

### 101 2.1 Historical data

102 This study uses observed time series measured in the climatological park of the Royal Mete-  
 103 orological Institute (RMI) at Uccle, near Brussels, Belgium. The data include time series of  
 104 observed precipitation [mm] from 1898–2002, and mean daily temperature  $T$  [°C] and daily refer-  
 105 ence evapotranspiration  $E$  [mm/day] from 1931–2002. The time series of  $E$  is derived using the  
 106 Penman-Monteith equation. The precipitation data have been recorded with a time resolution  
 107 of 10 min from 01/01/1898 to 31/12/2002 measured by a Hellmann–Fuess pluviograph (Démaré,  
 108 2003). This data set is quite unique in hydrology due to its extraordinary length with a sam-  
 109 pling frequency of 10 minutes. Its quality is ensured consistently at a high level by using the same  
 110 method of processing and measuring at the same location since 1898 (Ntegeka and Willems, 2008).  
 111 This time series has been used in several studies (Verhoest et al., 1997; Vaes and Berlamont, 2000;  
 112 De Jongh et al., 2006; Ntegeka and Willems, 2008; Vandenberghe et al., 2010; Vanhaute et al.,  
 113 2012; Pham et al., 2013; Willems, 2013; Pham et al., 2016) and is used to calibrate the rainfall  
 114 model as explained in Section 2.4. This time series has also been reprocessed to daily total pre-  
 115 cipitation [mm/day], further referenced to as  $P$ , for the period of 1931–2002, which is then used  
 116 together with the time series of  $T$  and  $E$  for the construction of different stochastic models.

### 117 2.2 Probability Distributed Model (PDM)

118 PDM is a lumped rainfall-runoff model which basically conceptualizes the absorption capacity of  
 119 soil in the catchment as a collection of three different storages (Moore, 2007; Cabus, 2008) (see  
 120 Fig. 1): i.e. (1) a probability distributed soil moisture storage ( $S_1$ ) based on a Pareto distribution  
 121 of soil moisture capacity to separate direct runoff  $Q_{dr}$  and subsurface runoff  $Q_{gr}$ ; (2) a surface  
 122 storage ( $S_2$ ) to transform direct runoff into surface runoff; and (3) a groundwater storage ( $S_3$ ) to  
 123 convert subsurface runoff to baseflow. The input for  $S_1$  is the net precipitation ( $P - E$ ), in which  
 124  $P$  and  $E$  are the precipitation and evapotranspiration, respectively. Further water loss from  $S_1$   
 125 may be due to  $Q_{dr}$  or  $Q_{gr}$ . The former is then converted to surface runoff  $Q_{ro}$  through surface  
 126 storage  $S_2$ , a fast response system involving a sequence of two linear reservoirs with small storage  
 127 time constants  $k_1$  and  $k_2$ . The direct runoff flow only happens when  $S_1$  is completely filled. The



128 recharge to the groundwater, controlled by the drainage time constant  $k_g$ , is transferred into base-  
 129 flow  $Q_{bf}$  through groundwater storage  $S_3$ , a slow non-linear response system with a large storage  
 130 time constant  $k_b$ . The sum of  $Q_{ro}$  and  $Q_{bf}$  equals the total discharge  $Q_t$ ; note that a constant  
 131 flow which presents any returns or abstractions to or from the catchment, represented by a par-  
 132 ameter  $q_{const}$ , also can be added. For a more detailed theoretical explanation and mathematical  
 133 description of the model, we refer to Moore (2007).

134  
 135 In this study, PDM is calibrated for the Grote Nete catchment using the Particle Swarm  
 136 Optimization algorithm (PSO) (Kennedy and Eberhart, 1995). This catchment, covering about  
 137 385 km<sup>2</sup> in the North of Belgium, has a maritime, temperate climate with an average precipi-  
 138 tation of about 800 mm/year (Vrebos et al., 2014). A time series of more than 6 years (from  
 139 13/8/2002–31/12/2008) at hourly time-step (precipitation, evapotranspiration and discharge) for  
 140 the catchment is available, in which the observations recorded during the period of 13/8/2002–  
 141 31/12/2006 are used for model calibration, while the remaining data (from 1/1/2007–31/12/2008)  
 142 are used for model validation.

## 144 2.3 Copula-based stochastic simulation of evapotranspiration and tem- 145 perature

### 146 2.3.1 Vine copulas

147 A copula is a multivariate function that describes the dependence structure between random  
 148 variables, independently of their marginal distributions (Sklar, 1959). The theorem of Sklar (Sklar,  
 149 1959) states that if  $F_{12}(x_1, x_2)$  is the joint distribution function of two random variables  $X_1$  and  
 150  $X_2$  with marginal cumulative distributions  $F_1$  and  $F_2$ , then there exists a bivariate copula  $C_{12}$   
 151 such that:

$$F_{12}(x_1, x_2) = C_{12}(F_1(x_1), F_2(x_2)) = C_{12}(u_1, u_2) \quad (1)$$

152 with  $u_1 = F_1(x_1)$  and  $u_2 = F_2(x_2)$ . For more theoretical details, we refer to Sklar (1959)  
 153 and Nelsen (2006).

154  
 155 The use of copulas allows to decompose the construction of a joint distribution function in  
 156 two independent steps, i.e. the modelling of the dependence structure and the modelling of the  
 157 marginal distribution functions (Nelsen, 2006; Salvadori and De Michele, 2007). As such, copulas  
 158 allow the use of complex marginal distribution functions (Salvadori et al., 2007). Because of this  
 159 advantage, the application of copulas is becoming more and more popular in hydrological and  
 160 meteorological studies. However, due to the complication in the construction of the copula model  
 161 for more than two variables, most research is limited to the bivariate case (Pham et al., 2016).

162  
 163 A flexible construction method for high-dimensional copulas, known as the vine copula con-  
 164 struction, has been introduced in the work of Bedford and Cooke (2001, 2002), in which multivari-  
 165 ate copulas are built by decomposing the multivariate density into a product of bivariate copula  
 166 densities. Vine copulas constitute two main advantages. First, they are simple and straightfor-  
 167 ward to apply. Second, they are very flexible and have the ability to model all types of dependence  
 168 because the bivariate copulas can be selected from a wide range of copula families (Kurowicka and  
 169 Cooke, 2007; Aas et al., 2009; Czado, 2010).

170  
 171 There is, however, a large number of possible decompositions for the construction of vine  
 172 copulas (Aas et al., 2009); for example, there are 24 and 240 different constructions of vine copulas  
 173 for the four- and five-dimensional case, respectively (Aas et al., 2009). Examples of two regular  
 174 four-dimensional vine copulas are given in Fig. 2(a, b). One usually focuses on two special types  
 175 of regular vine copulas: Canonical vine copulas (C-vine copulas) and D-vine copulas (Kurowicka  
 176 and Cooke, 2007). If all mutual dependences involve the same variable, the construction yields a  
 177 C-vine copula (Fig. 2(c)). If all mutual dependences are considered one after the other, i.e. the  
 178 first with the second, the second with the third, the third with the fourth, etc., the construction

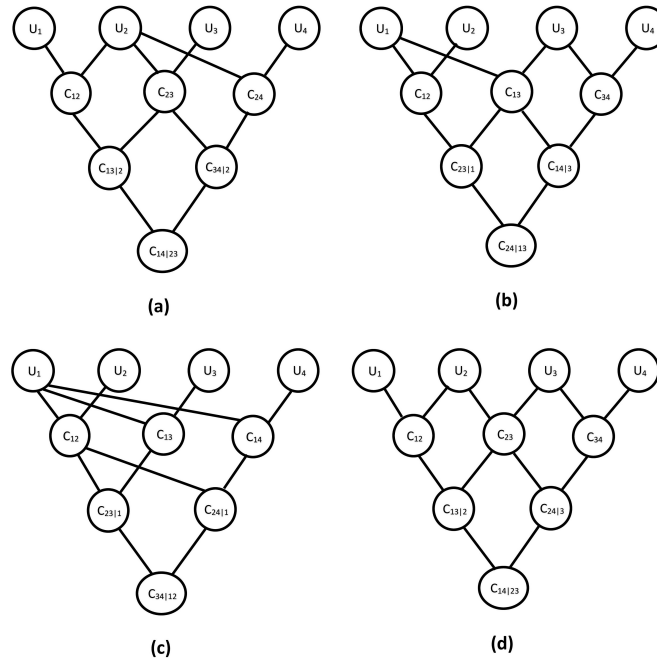


Figure 2: Examples of four-dimensional vine copulas: (a, b) regular vine copulas, (c) canonical vine or C-vine copula, (d) D-vine copula.

179 yields a D-vine copula (Fig. 2(d)). Since because C-vine copulas are easier to construct than D-  
 180 vine copulas, the former are selected in this study for the constructions of copula-based generators  
 181 of temperature and evapotranspiration. More details of the construction and simulation from a  
 182 C-vine copula are given in the work of Aas et al. (2009).

### 183 2.3.2 Copula-based stochastic simulation of evapotranspiration

184 In order to generate stochastic time series of evapotranspiration, we make use of the vine-copula-  
 185 based approach proposed in the work of Pham et al. (2016) in which C-vine copulas are used to  
 186 describe the dependences between evapotranspiration and other variables, such as temperature,  
 187 precipitation and dry fraction within a day. The advantage of the method is that the statistical  
 188 properties of the evapotranspiration time series and the dependence structures between evapo-  
 189 transpiration and other variables are well maintained. Furthermore, the model construction and  
 190 simulation are simple to apply. After comparing the results of different vine models, Pham et al.  
 191 (2016) found that the best simulations of daily evapotranspiration were provided by the four-  
 192 dimensional C-vine copula  $V_{TPDE}$  relating daily temperature ( $T$ ), precipitation ( $P$ ), dry fraction  
 193 ( $D$ ) and evapotranspiration ( $E$ ), and the three-dimensional C-vine copula  $V_{TPE}$  relating  $T$ ,  $P$   
 194 and  $E$ . As there is no major difference in performance between simulations using  $V_{TPDE}$  and  
 195  $V_{TPE}$  (Pham et al., 2016), for simplicity, we consider to use only  $V_{TPE}$  in which the Frank copula  
 196 family is selected for modelling the dependences between variables. As shown in (Pham et al.,  
 197 2016), the White goodness-of-fit test (Schepsmeier, 2015) indicated that the Frank copula family  
 198 allows for describing the dependence structure of the data included in the  $V_{TPE}$ . In order to avoid  
 199 the seasonal effects, a different C-vine copula model is used for each month. More details on the  
 200 comparison of several evapotranspiration copula-based models can be found in Pham et al. (2016).

201  
 202 The construction of  $V_{TPE}$  is given as follows (see Fig. 3(a)). First, values  $(u_{T,j}, u_{P,j}, u_{E,j})$  of

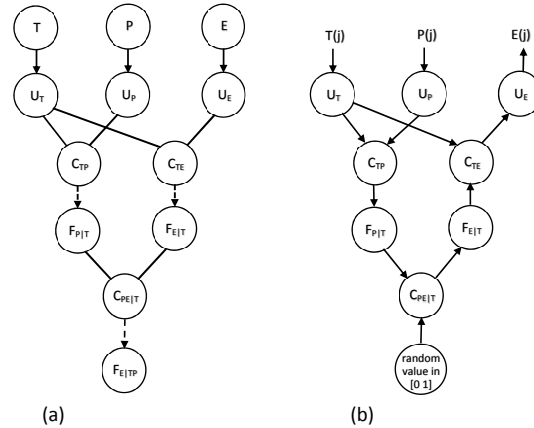


Figure 3: Construction of C-vine copula  $V_{TPE}$  (a) and simulation of  $E$  from  $V_{TPE}$  (b)

203  $U_T$ ,  $U_P$  and  $U_E$  are derived from the marginal distributions of respectively  $T$ ,  $P$  and  $E$  ( $j = 1, \dots, n$   
 204 and  $n$  is the number of data points), and are used to select and fit the bivariate copulas  $C_{TP}$  and  
 205  $C_{TE}$ , respectively. These bivariate copulas are conditioned on  $U_T$  through partial differentiation,  
 206 resulting in the conditional cumulative distribution functions  $F_{P|T}$  and  $F_{E|T}$ . Using these two  
 207 conditional distributions, the conditional probabilities are calculated for all data points. To these  
 208 probabilities, which are also uniformly distributed on  $[0,1]$ , a bivariate copula  $C_{PE|T}$  is fitted, of  
 209 which the partial derivative to  $F_{P|T}$  can be computed to obtain  $F_{E|TP}$ . Once the C-vine copula  
 210 model is fitted, a corresponding time series of evapotranspiration values can be generated, for a  
 211 given time series of rainfall and temperature data, by sampling the copula (Fig. 3(b)). To that  
 212 end, values of  $U_E$  are calculated as:

$$u_E = F_{E|T}^{-1}(F_{E|TP}^{-1}(r|u_T, u_P)) \quad (2)$$

213 where  $r$  is a random value drawn from a uniform distribution on  $[0,1]$ . Then the corresponding  
 214 evapotranspiration value  $e$  can be calculated using the inverse marginal distribution function:

$$e = F_E^{-1}(u_E) \quad (3)$$

215 It is clear that the values of  $U_E$  are affected by the random value  $r$ , therefore, several simulations  
 216 will show some variability. To account for these stochastic effects, the simulation was repeated  
 217 100 times. Figure 4 displays the comparisons between frequency distributions of observed and  
 218 simulated evapotranspiration obtained by  $V_{TPE}$  for the different months. From these plots, it  
 219 can be seen that the frequency distributions of the stochastic evapotranspiration are very similar  
 220 to those of the reference evapotranspiration in Uccle (red line). In order to assess whether the  
 221 dependence structures between simulated evapotranspiration and other variables are maintained,  
 222 for each of the 100 simulations, the mutual dependences between  $E$  and the other variables,  $T$   
 223 or  $P$ , were assessed via Kendall's tau for each month. Figure 5 shows box plots of the obtained  
 224 values of Kendall's tau for  $E$  vs.  $T$  and  $E$  vs.  $P$  dependences for 100 simulations. These figures  
 225 show that, in general, the observed dependences between both  $E$  vs.  $T$  and  $E$  vs.  $P$  are preserved  
 226 with the stochastic simulated evapotranspiration.

### 227 2.3.3 Copula-based stochastic simulation of temperature

228 Temperature data are required for the stochastic modelling of evapotranspiration. However, in  
 229 situations where no long-term time series of temperature is available, it is necessary to use a  
 230 stochastically-generated temperature time series. We use a similar approach as Pham et al.  
 231 (2016) to develop a stochastic temperature model based on copulas. This model makes use of

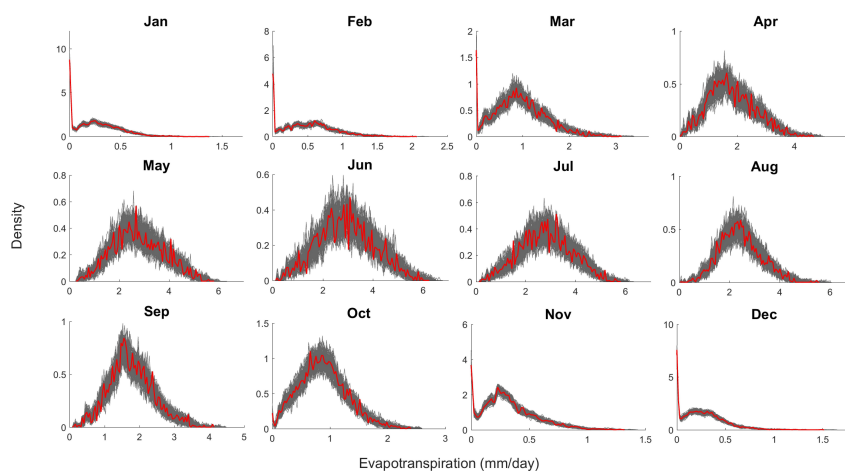


Figure 4: Comparison between the frequency distributions of evapotranspiration of observed and simulated values: Uccle (red), the ensemble of 100 time series simulated using the C-vine copula  $V_{TPE}$  (grey).

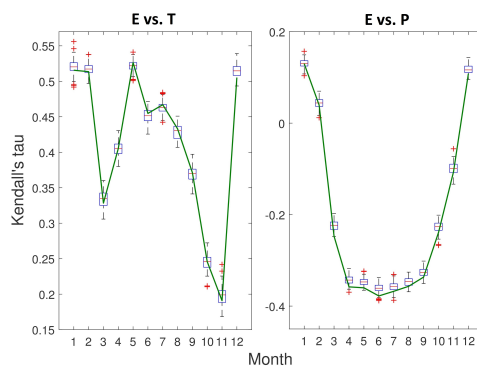


Figure 5: Comparison between Kendall's tau for the relations of  $E$  vs.  $T$  (left) and  $E$  vs.  $P$  (right) of observed and simulated values: Uccle (green line), 100 simulated time series (box plot)

232 the dependence between the temperature and the precipitation of the same day (i.e. at day  $j$ ) and  
 233 the temperature of the previous day (i.e. at day  $j - 1$ ). Firstly, the correlation between the tem-  
 234 perature at day  $j$  ( $T_j$ ) and the temperature at the previous day ( $T_{j-1}$ ) is assessed by the Pearson  
 235 correlation coefficient. Given the high correlation, i.e. 0.94, we thus can conclude that there is a  
 236 strong dependence between  $T_j$  and  $T_{j-1}$ . Similarly as for the stochastic evapotranspiration model,  
 237 a C-vine copula is employed in which  $T_{j-1}$  is chosen as the core variable. The model is referred  
 238 to as  $V_{T_p,PT}$ , where  $T_p$  refers to the temperature of the previous day.

239  
 240 The construction procedure of  $V_{T_p,PT}$  is similar to the one of  $V_{TPE}$  (see Section 2.3.2). The  
 241 simulation process of the temperature model is different from that of the evapotranspiration model,  
 242 in the sense that it requires a modelled input from the previous time step (i.e.  $T_p$ ) in order to  
 243 generate a new value for  $T$ . The simulation algorithm of  $T$  can be performed as follows:



Table 1: Bivariate copulas selected by AIC for  $V_{T_pPT}$ , where F stands for Frank, Ga for Gaussian, G for Gumbel, C for Clayton and J for Joe

Month	$V_{T_pPT}$		
	$C_{T_pP}$	$C_{T_pT}$	$C_{PT T_p}$
Jan	F	Ga	F
Feb	F	Ga	Ga
Mar	F	Ga	F
Apr	F	Ga	F
May	F	Ga	F
Jun	F	Ga	F
Jul	F	Ga	F
Aug	F	Ga	F
Sep	F	Ga	Ga
Oct	C	Ga	Ga
Nov	C	Ga	F
Dec	F	Ga	F

$$u_T = F_{T|T_p}^{-1}(F_{T|T_p}^{-1}(F_{T|T_p}^{-1}(r|u_{T_p}, u_P))) \quad (4)$$

$$t = F_T^{-1}(u_T) \quad (5)$$

244 In order to maintain the dependence structures between variables, but still keep the model  
 245 simple and easy to construct, the best bivariate copulas for the C-vine copula are chosen using  
 246 the Akaike's information criterion (AIC) (Akaike, 1973) from five one-parameter copula families,  
 247 i.e. the Gaussian, the Clayton, the Gumbel, the Frank and the Joe family. Table 1 illustrates  
 248 which copulas were selected. This table shows that the Frank copula family is often selected for  
 249  $C_{T_pP}$  and  $C_{PT|T_p}$ , while the Gaussian copula is often chosen for  $C_{T_pT}$ . To keep the copula-based  
 250 simulation procedure simple, we restrict the model to use only a combination of Frank-Gaussian-  
 251 Frank for the C-vine copula  $V_{T_pPT}$ . Further, the White goodness-of-fit test (Schepsmeier, 2015) is  
 252 applied to check whether the dependence present in the data is captured by the Frank-Gaussian-  
 253 Frank C-vine copulas. With  $p$ -values larger than 0.05 for all months, we find that the dependence  
 254 structure of the data can be described by the selected copulas. These copulas are then used for  
 255 generating temperature given the time series of precipitation.

256  
 257 To assess the performance of the model, the statistics of 100 stochastic time series of tem-  
 258 perature using the observed daily precipitation from 1931 to 2002 are compared to those of the  
 259 observations. The empirical cumulative distribution functions (ECDF) of the monthly mean tem-  
 260 perature for each of the simulated 72-year time series are shown in Fig. 6. The statistics of  
 261 the simulations seem to be relatively similar to the observations. Figure 7 shows the monthly  
 262 maximum temperature of the ensemble and of the observed temperature series corresponding to  
 263 empirical return periods. This figure shows that the extremes are well modelled for all months.



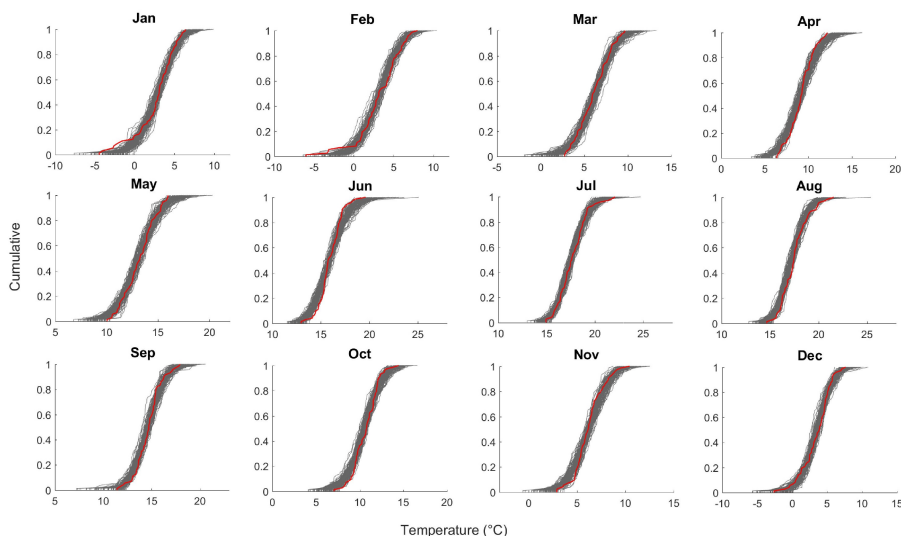


Figure 6: Comparison between the empirical cumulative distribution function (ECDF) of the monthly mean  $T$  of the observed and simulated values: Uccle (red), the ensemble of 100 time series simulated using the C-vine copula  $V_{TpPT}$  (grey).

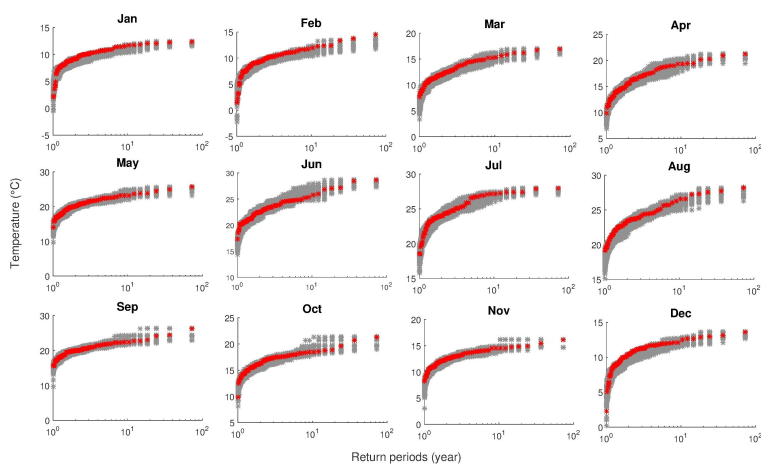


Figure 7: Comparison between the return periods of monthly extremes of the observed and simulated temperature values: Uccle (red), the ensemble of 100 time series simulated using the C-vine copula  $V_{TpPT}$  (grey).



Table 2: Optimal parameter set for the (monthly) MBL model.

Parameter	$\lambda$	$\kappa$	$\phi$	$\mu_x$	$\alpha$	$\nu$
January	0.021	0.009	0.002	11.037	12.042	0.833
February	0.014	0.008	0.001	15.000	4.041	0.143
March	0.018	0.009	0.001	15.000	5.393	0.219
April	0.017	0.151	0.032	0.823	20.000	19.029
May	0.023	1.130	1.000	0.371	4.000	14.420
June	0.016	0.089	0.059	1.190	10.064	20.000
July	0.012	0.012	0.004	7.676	20.000	5.715
August	0.010	0.003	0.001	15.000	19.963	2.729
September	0.014	0.199	0.100	0.417	4.000	14.039
October	0.013	8.949	0.096	0.095	4.000	2.488
November	0.023	0.121	0.026	1.061	4.000	2.486
December	0.014	0.005	0.001	14.998	20.000	1.792

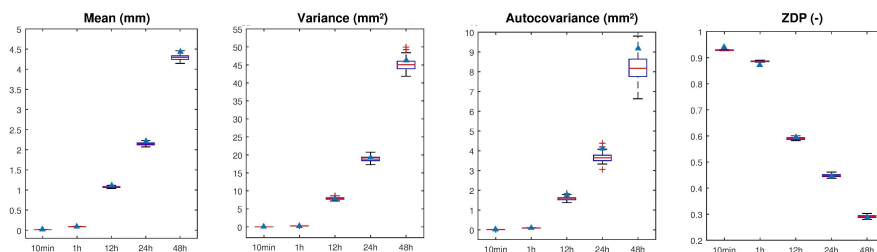


Figure 8: Comparison between observed and simulated precipitation data for the mean, variance, autocovariance and zero-depth probability (ZDP): Uccle (blue triangle), the ensemble of 100 simulated time series by the MBL model (box plot).

## 264 2.4 Simulated precipitation by the MBL model

265 In situations where no long time series of precipitation is available, one can use a stochastic rainfall  
 266 model. In this study, the modified Bartlett–Lewis (MBL) model (Rodriguez-Iturbe et al., 1988) is  
 267 selected to generate the precipitation time series based on the results from Pham et al. (2013) in  
 268 which the MBL model is considered to be the best version of the different BL models tested on the  
 269 Uccle data set. The MBL model is calibrated based on the mean, variance, lag-1 autocovariance and  
 270 zero-depth probability (ZDP) at the aggregation levels of 24 h, 48 h and 72 h instead of 10  
 271 min, 1 h and 24 h that were used in Pham et al. (2013). The reason for only selecting aggregation  
 272 levels of at least one day is to consider situations where only daily precipitation data would be  
 273 available. The values of the calibrated parameters are given in Table 2. Details of the MBL model  
 274 and the model calibration are provided by Pham et al. (2013). The stochastic rainfall time series  
 275 is simulated at the same 10-minute time resolution as the observations. In order to assess the per-  
 276 formance of the model, the abilities of the model to reproduce some general historical statistics,  
 277 such as mean, variance, the lag-1 autocovariance and ZDP, at aggregation levels of 10 min,  
 278 12 h, 24 h and 48 h are investigated based on an ensemble of 100 time series.

279  
 280 In Fig. 8, some general statistics at different aggregation levels are compared for 100 time series  
 281 obtained by the MBL model and the observed time series in Uccle. In order to further unveil the  
 282 behaviour of the model, the general statistics are calculated at different aggregation levels for each  
 283 year and presented in the form of an ECDF (Fig. 9). From both figures, it can be seen that the  
 284 mean is generally reproduced well by the model at all levels of aggregation. At the sub-hourly  
 285 level, the variance and autocovariance are slightly overestimated. For higher aggregation levels,  
 286 an increasing variation is found for both statistical properties. At higher levels of aggregation,  
 287 the ZDP is similar to that found for the observed time series, whereas for hourly and sub-hourly

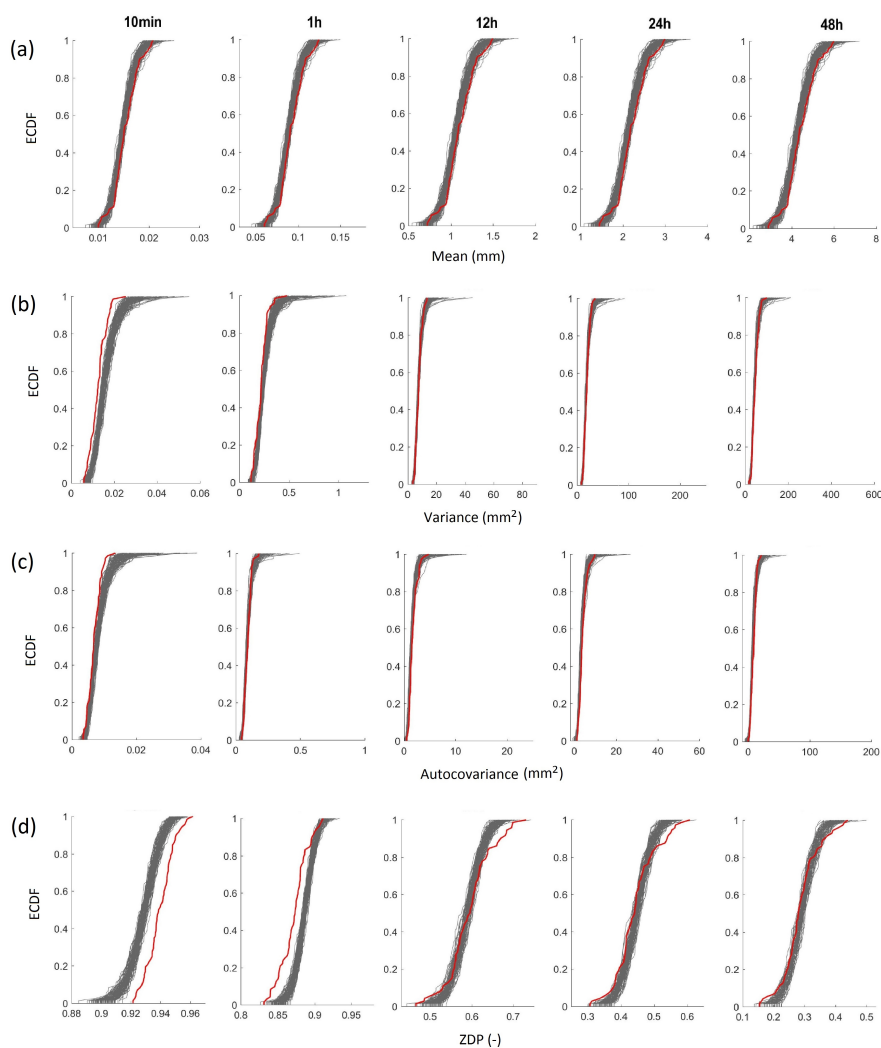


Figure 9: Comparisons between the empirical cumulative distribution function of mean, variance, autocovariance and ZDP calculated for the observed and simulated precipitation data for different aggregation levels for each year: Uccle (red), 100 simulated time series by the MBL model (grey). ECDFs are shown for the (a) mean, (b) variance, (c) lag-1 autocovariance and (d) the zero-depth probability (ZDP).

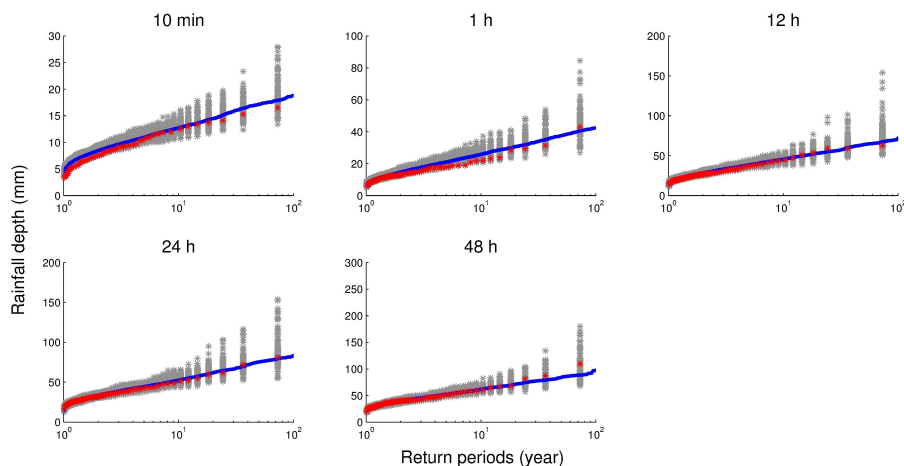


Figure 10: Comparisons between the return periods of the observed and simulated precipitation data at different aggregation levels: Uccle (red), the ensemble of 100 simulated time series by the MBL model (grey). Calculation of the extremes for a given return period on a time series that is based on concatenating the 100 simulated time series, results in the blue line

288 levels, a slight deviation in ZDP-values are found with respect to the observations.

289

290 Figure 10 shows the empirical univariate return periods of the annual maximum rainfall depths  
291 of the observed and simulated series, considering five different aggregation levels. Compared to the  
292 observations, it seems that the MBL model is able to preserve the maxima at all aggregation levels.  
293 It can be seen in this study that the MBL model does not suffer from the problem of underestimation  
294 of extreme values at sub-hourly aggregation levels that were reported in the work of Verhoest  
295 et al. (1997) and Cameron et al. (2000). From the analysis, it seems that the MBL model is  
296 capable of preserving the sub-daily statistics even though the calibration procedure only included  
297 daily and multi-day statistics. Yet, further research is needed for exploring this improved behavior.

298

299 Figure 10 also shows that a large variation in extreme values is found for larger return periods.  
300 The MBL model allows for generating rainfall time series mimicking the statistics of the observed  
301 series. Due to its structure, the modeled precipitation values are not restricted to the range of  
302 rainfall values in the observations, making this model able to generate rainfall events having a  
303 return period larger than the observed time series. Yet, it can thus be expected that within  
304 the modeled time series of 72 years, events may occur having a true return period that is larger  
305 than the length of the modeled time series. If longer time series would be simulated, a better  
306 estimation of the rainfall corresponding to return periods that are smaller than the observed time  
307 series should be obtained. To demonstrate this, all 50 series generated are concatenated, resulting  
308 in one time series of  $50 \times 72 = 3600$  years, for which the return periods are calculated empirically  
309 and plotted (only for return periods less than 100 years) as a blue line in Figure 10. As can be seen  
310 for return periods smaller than 100 years, a good fit with the observations are obtained, showing  
311 that MBL is capable of reproducing extremes. Yet, the user should use much longer time series  
312 than the maximum return period aimed for.

### 313 3 Discharge simulation scenarios

314 The catchment discharge is calculated by the PDM that uses precipitation and evapotranspiration  
315 data as inputs. In order to assess the impact of each stochastic variable on the modelling of discharge,  
316 discharge, three cases have been developed that can be compared to a reference situation (cfr. Fig. 11).

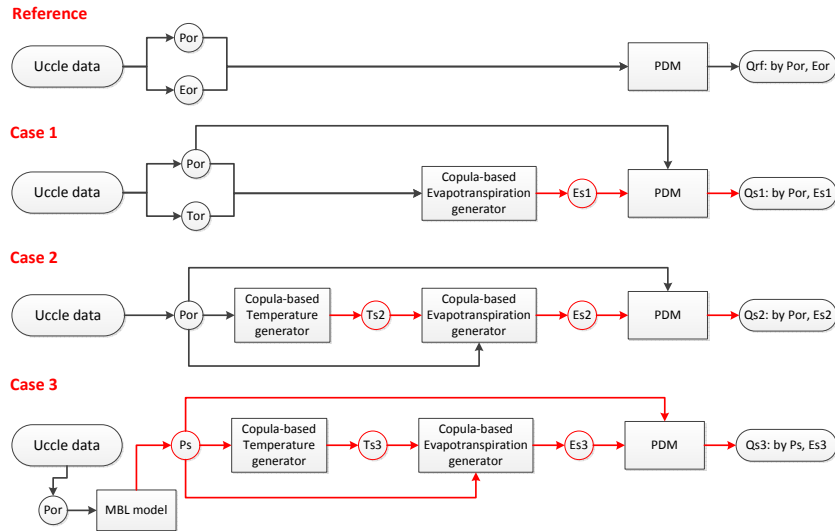


Figure 11: Different cases for discharge simulation.  $P_{or}$ ,  $E_{or}$  and  $T_{or}$  refer to the observed time series.  $P_s$ ,  $E_{s1}$ ,  $E_{s2}$ ,  $E_{s3}$ ,  $T_{s2}$  and  $T_{s3}$  refer to the simulated time series (red block). Red arrows indicate the simulation processes related to stochastically-generated time series.

317 The reference situation is obtained by running the PDM with the observed time series of precipi-  
 318 tation and evapotranspiration. In case 1, it is supposed that insufficient evapotranspiration data  
 319 would be available (e.g. a shorter time series than the observed precipitation), the stochastic evap-  
 320 ottranspiration can then be generated using the three-dimensional C-vine copula, i.e.  $V_{TPE}$ , given  
 321 observed rainfall and temperature. The simulation is repeated 50 times in order to account for  
 322 stochastic effects. In case 2, where only a sufficient long time series of precipitation is available, the  
 323 process starts with temperature simulations, then evapotranspiration can be modelled using the  
 324 observed precipitation and stochastically-generated temperature using the  $V_{TPE}$  copula. As pre-  
 325 sented before, temperature values will be generated by the three-dimensional C-vine copula  $V_{T_pPT}$   
 326 that relates temperature  $T$  to daily precipitation  $P$  and the daily temperature of the previous day  
 327  $T_p$ . To account for stochastic effect, 50 time series of temperature are generated. Next, each of  
 328 50 time series of temperature, together with the observed precipitation data, are used to simulate  
 329 50 corresponding time series of evapotranspiration. Therefore, in total 2500 time series of evap-  
 330 ottranspiration are generated. Case 3 accounts for a situation in which data would insufficiently be  
 331 available for all input variables. In this case, an ensemble of 50 time series of precipitation could  
 332 be generated using the MBL model. For each of these time series, 50 time series of temperature  
 333 and 2500 time series of evapotranspiration can be obtained using the same approach in case 2.  
 334 In total, 125000 time series of evapotranspiration are generated in case 3. In order to construct  
 335 copula models and evaluate discharge simulations in all cases, this study uses the same time series  
 336 of precipitation, evapotranspiration and temperature at Uccle. In all cases, discharge is simulated  
 337 using the PDM that was calibrated for the Grote Nete catchment in Belgium (see Section 2.2).  
 338 By this approach, the uncertainty due to the PDM can be partly excluded from the study, i.e. we  
 339 study the change in performance with respect to the reference situation. It makes sense because  
 340 the three cases use exactly the same PDM, a similar uncertainty due to the model is assumed for  
 341 all cases as for the reference situation. Therefore, the change in performance for all cases with  
 342 respect to the reference situation can be attributed to the differences in inputs to the model. The  
 343 discharge simulations in the three cases are denoted as  $Q_{s1}$ ,  $Q_{s2}$  and  $Q_{s3}$ , respectively, while the  
 344 reference discharge is denoted by  $Q_{rf}$ .

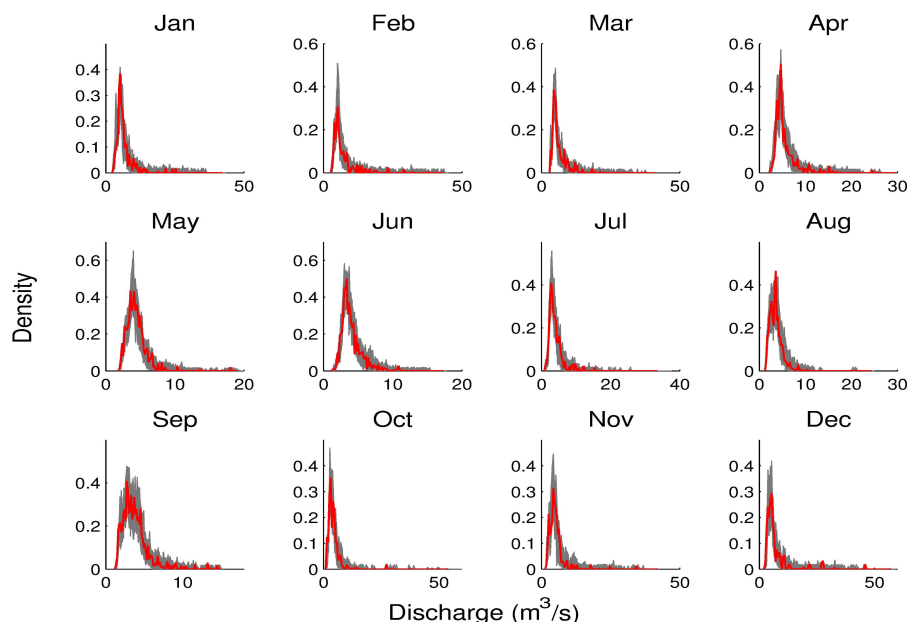


Figure 12: Comparison between the frequency distributions of the reference discharge  $Q_{rf}$  (red) and the ensemble of 50 time series of discharge values simulated using observed precipitation and simulated evapotranspiration values in case 1 (grey).

## 345 4 Results and discussions

### 346 4.1 Case 1

347 The catchment discharge can be simulated by means of the PDM that uses precipitation and  
 348 evapotranspiration data. In case 1 (cfr. Fig. 11), where only daily observed precipitation and  
 349 temperature data are available, 50 stochastically-generated evapotranspiration time series are  
 350 generated using the three-dimensional C-vine copula  $V_{TPE}$ . The results shown in Section 2.3.2  
 351 and the work of Pham et al. (2016) reflect that the C-vine copula  $V_{TPE}$  performs well and its  
 352 simulations lie very close to the values of the observed evapotranspiration. Figure 12 displays the  
 353 comparison between the frequency distributions of  $Q_{rf}$  and  $Q_{s1}$  for the different months. It can  
 354 be seen that the distributions of  $Q_{s1}$  are quite similar to those of the reference discharge for all  
 355 months. For a further analysis of mean discharges and annual extremes of  $Q_{s1}$ , we refer to Section  
 356 4.3.

### 357 4.2 Case 2

358 In case 2 (cfr. Fig. 11), only a time series of precipitation of sufficient length is available and the  
 359 temperature values are simulated using the C-vine copula  $V_{TpPT}$ . The observed precipitation and  
 360 stochastically-generated temperature values are then used for reproducing the evapotranspiration  
 361 by means of the C-vine copula  $V_{TPE}$ . Through comparing the results of this case with that of  
 362 case 1, we can assess the impact of introducing a stochastic temperature model on the modelled  
 363 evapotranspiration time series and the modelled discharge.

364  
 365 As shown in Section 2.3.3 and Fig. 13, the stochastically-generated temperature data gener-  
 366 ated by the C-vine copula  $V_{TpPT}$  model are reliable and can be used together with the recorded  
 367 precipitation to simulate 2500 time series of evapotranspiration in the next step (i.e. for each tem-

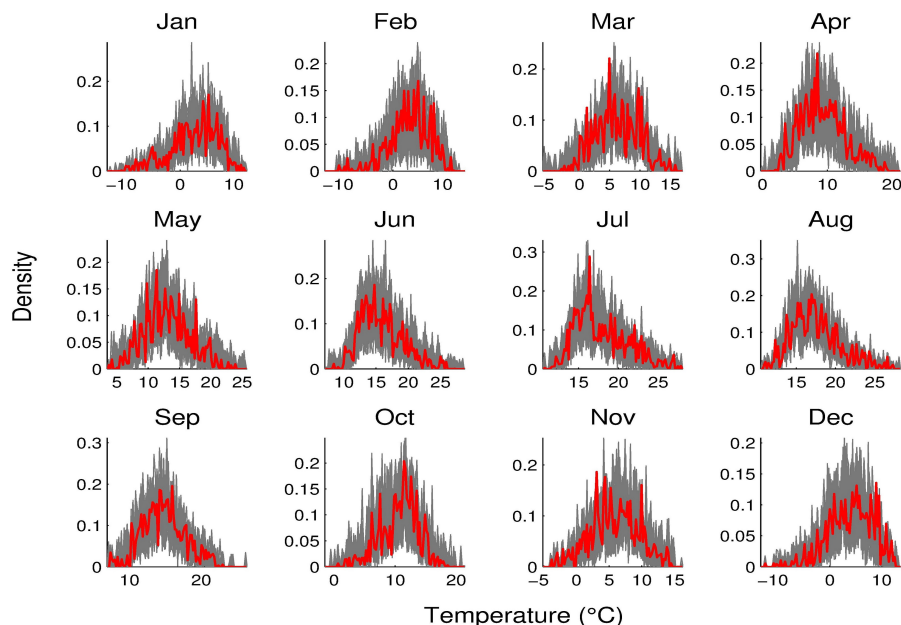


Figure 13: Comparison between the frequency distributions of temperature of the observed and simulated values in case 2: Uccle (red), the ensemble of 50 time series simulated using the C-vine copula  $V_{T_p,PT}$  (grey).

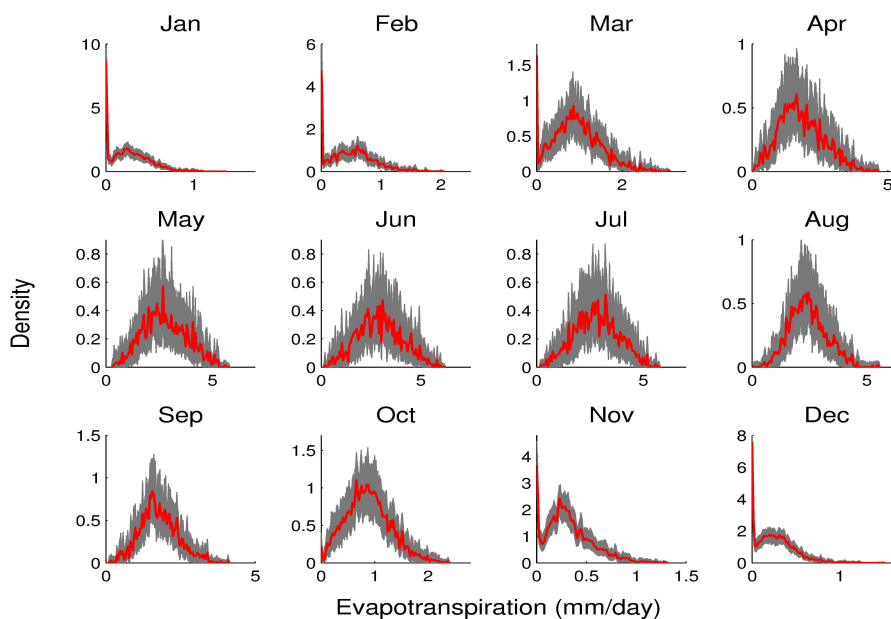


Figure 14: Comparison between the frequency distributions of evapotranspiration of the observed and simulated values in case 2: Uccle (red), the ensemble of 2500 time series simulated using the C-vine copula  $V_{TPE}$  (grey).

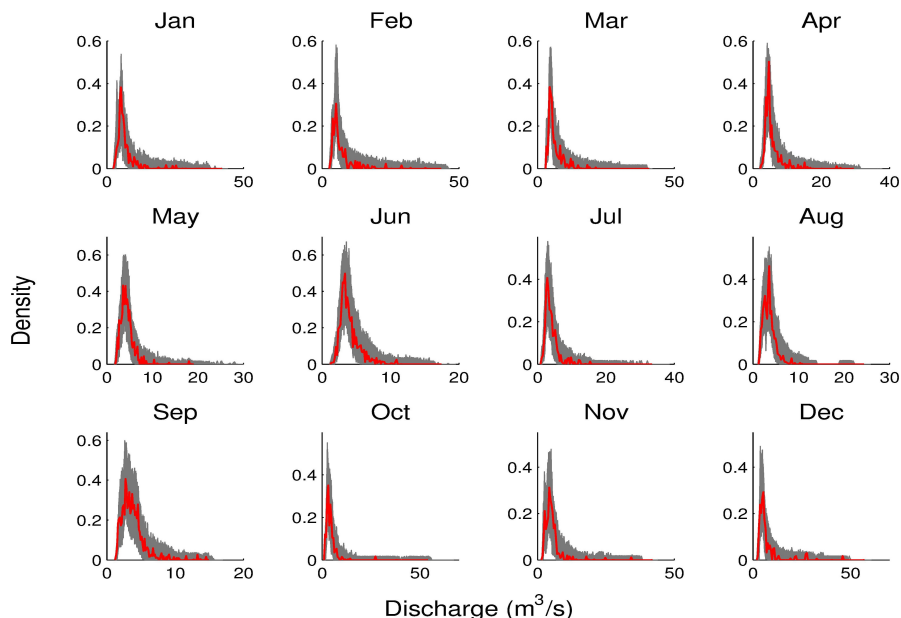


Figure 15: Comparison between the frequency distributions of reference discharge (red) and the ensemble of 2500 time series of discharge values simulated using the observed precipitation and simulated evapotranspiration in case 2 (grey).

368 perature series, 50 evapotranspiration series are generated). The frequency distributions of the  
 369 2500 time series of the simulated evapotranspiration are shown in Fig. 14. It can be seen from the  
 370 figures that these distributions are similar to those of the observations in Uccle and those of the  
 371 modelled evapotranspiration in case 1 for all months. Figure 15 displays a comparison between  
 372 the frequency distributions of the simulated discharge ( $Q_{s2}$ ) and the reference discharge ( $Q_{rf}$ ).  
 373 In general, the grey areas representing 2500 simulated time series are slightly wider than those in  
 374 case 1. We conclude that the introduction of stochastically-generated temperature does not cause  
 375 considerable deviations in the simulation of evapotranspiration and discharge.

### 376 4.3 Case 3

377 This case accounts for a situation in which no time series (of sufficient length) are available as  
 378 shown in Fig. 11. The first step consists of generating 50 time series of precipitation by means of  
 379 the MBL model (see Section 2.4) and aggregating these to the daily level. Then, each of those time  
 380 series is used for modelling 50 time series of temperature, each used for generating 50 evapotranspiration  
 381 series. Therefore, in total 125000 time series of evapotranspiration are generated. Finally,  
 382 125000 time series of the catchment discharge are simulated using the stochastically-generated  
 383 time series of precipitation and corresponding evapotranspiration values. This case will allow for  
 384 assessing the uncertainty introduced by using the MBL model for generating precipitation values  
 385 as input to a rainfall-runoff model.

386  
 387 First, the simulated time series of precipitation are used as inputs to the C-vine copula  $V_{T_p,PT}$   
 388 to generate time series of temperature. The modelled copula-based temperature values are compared  
 389 with the observed temperature in Uccle in terms of the frequency distributions in Fig. 16.  
 390 From these figures, it can again be seen that the distributions of the simulations follow those of  
 391 the observations. With respect to the frequency distributions, the simulated evapotranspiration  
 392 (Fig. 17) in this case is similar to the observed evapotranspiration, but more deviations can be





393 observed in this case than in the previous cases. The modelled time series of precipitation and  
394 evapotranspiration are then used for modelling the discharge. The frequency distributions of the  
395 simulated discharge values for the different months are displayed in Fig. 18. From the differ-  
396 ent plots, it can be concluded that the simulations still follow the distribution of the reference  
397 discharge (red line).

398 Compared to the simulated discharge of cases 1 and 2, more higher extreme values are generated  
399 and the grey areas representing the ensemble of 125000 time series are generally wider, indicating  
400 that mainly the stochastic generation of precipitation has introduced considerable variations into  
401 the discharge simulations. This increase in uncertainty should however be treated with care.  
402 As stated before, the generated rainfall series may include extremes that are larger than the  
403 ones in the observed time series. Such large precipitation values will inevitably result in a large  
404 surface runoff production causing extreme discharges. The large variability in extreme rainfall as  
405 observed in Figure 10 will consequently lead to large variabilities in modeled extreme discharges  
406 (cfr. Figure 19). If, however, the discharge extremes from a longer time series are studied, the  
407 variation in extremes is strongly reduced. To demonstrate this, 50 rainfall time series of 3600 year  
408 and corresponding evapotranspiration time series (remark that only one series is generated per  
409 rainfall time series) are used as input to the rainfall-runoff model, and the extremes, having return  
410 periods smaller than 500 years, are plotted for each of these 50 time series (Figure 20). As can  
411 be seen, the large uncertainties in extremes, encountered when using 72 year time series as input,  
412 are highly reduced, showing a slight overestimation for larger return periods, if compared to those  
413 modeled using the observed time series of rainfall and evapotranspiration. Yet, it is impossible to  
414 state whether true overestimations are obtained, or that, due to the stochastic nature or rainfall  
415 (and evapotranspiration), the observations used never resulted in extreme discharge events that  
416 actually exceed a (true) 40-year return period event (i.e., the maximum discharge based on the  
417 observed time series of precipitation and evapotranspiration corresponds to a return period of  
418 about 40 years based on the simulations using the modelled very long time series of precipitation  
419 and evaporation). Similarly as discussed for Figure 10, this result makes a plea for using modeled  
420 discharge time series of a length that is a multiple of the maximum return period of discharge  
421 aimed at, where longer time series reduce the variation in discharge values at high return periods  
422 at the expense of run-time. Further research will be needed to seek for the trade-off between  
423 length of the time series and the remaining uncertainty.

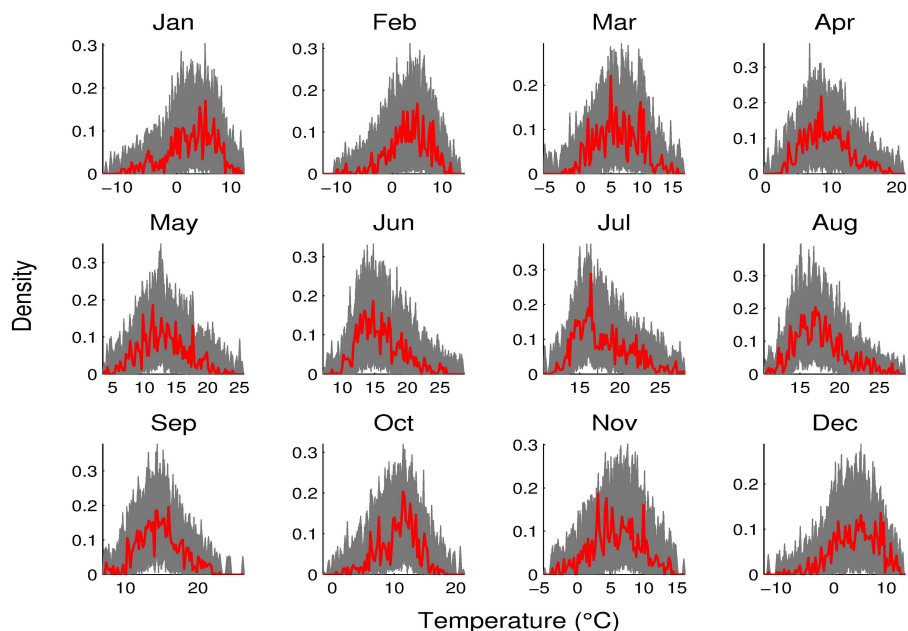


Figure 16: Comparison between the frequency distributions of temperature of the observed and simulated values in case 3: Uccle (red), the ensemble of 2500 time series simulated using the C-vine copula  $V_{TPPT}$  (grey).

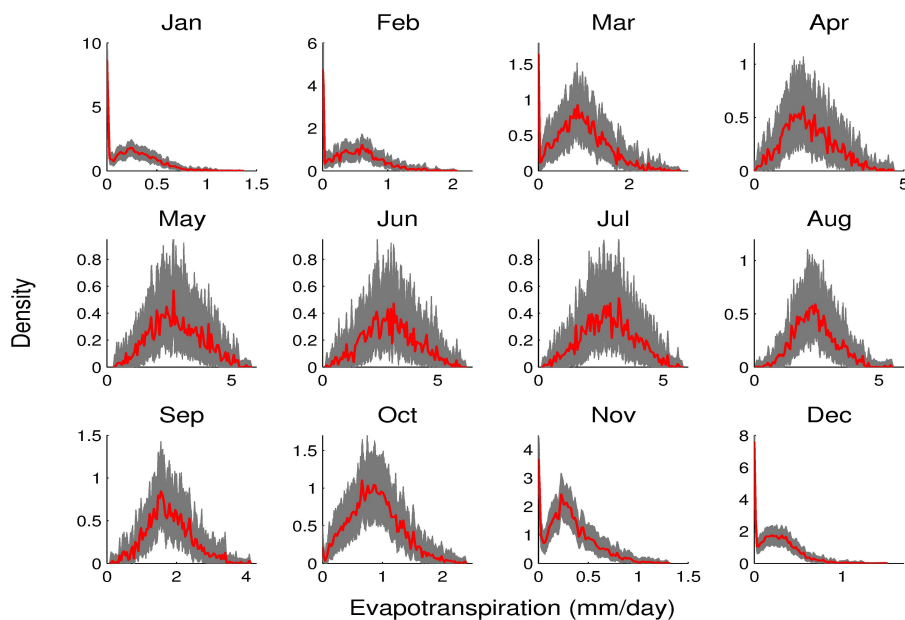


Figure 17: Comparison between the frequency distributions of evapotranspiration of the observed and simulated values in case 3: Uccle (red), the ensemble of 125000 time series simulated using the C-vine copula  $V_{TPE}$  (grey).

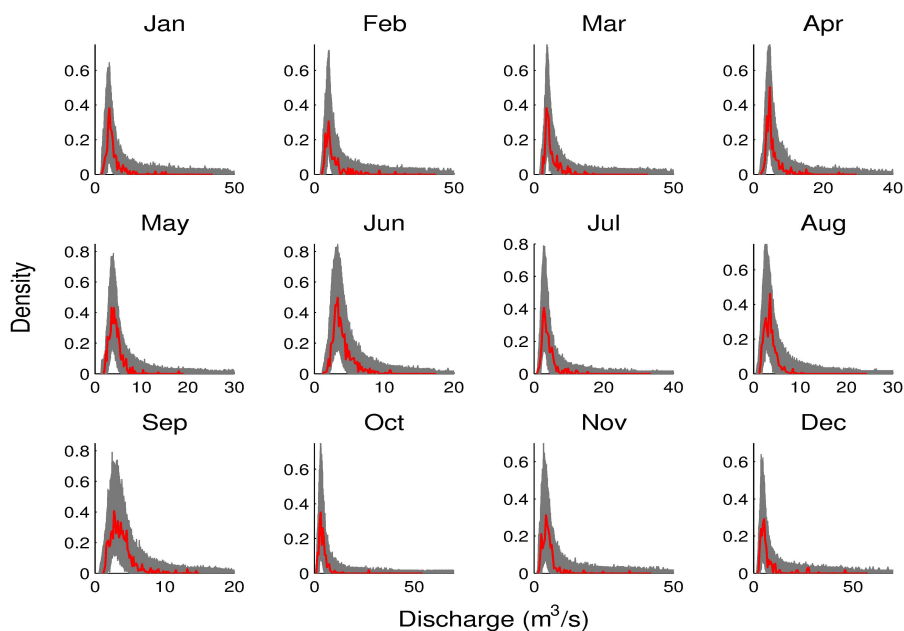


Figure 18: Comparison between the frequency distributions of reference discharge  $Q_{rf}$  (red) and the ensemble of 125000 time series of discharge values simulated using the simulated precipitation and evapotranspiration in case 3 (grey).

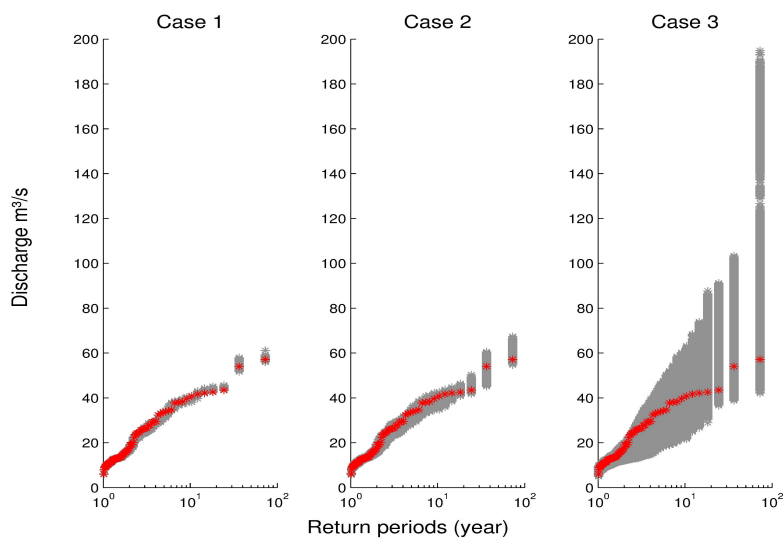


Figure 19: Comparison between the empirical return periods of annual extremes of the observed and simulated discharge for all cases: reference discharge  $Q_{rf}$  (red), the ensemble of time series of simulated discharge (grey).

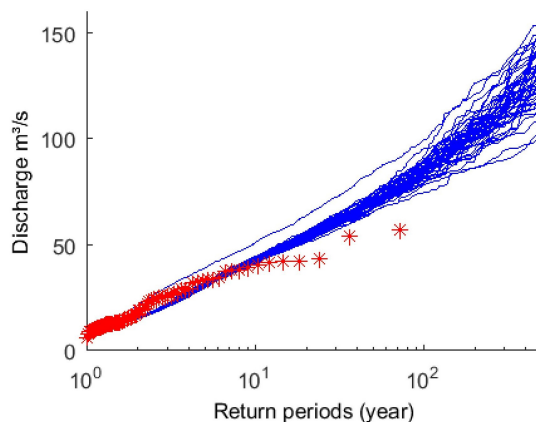


Figure 20: Comparison between the empirical return periods of annual extremes of the observed and simulated discharge for case 3 based on 50 time series of 3600 years of rainfall and corresponding evapo-transpiration.

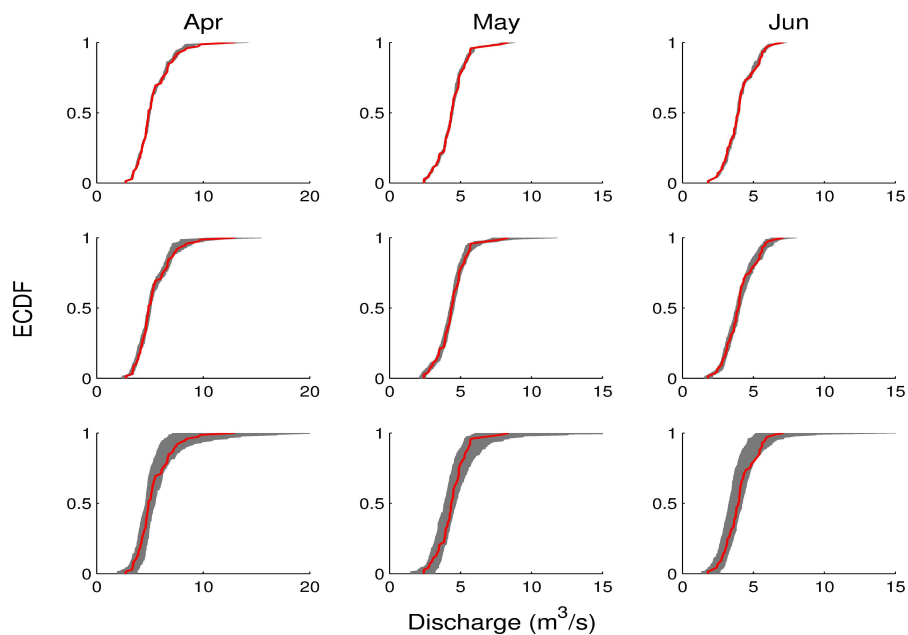


Figure 21: Comparison between the ECDF of the mean of discharge for Apr - Jun of the observed and simulated values in three cases: reference discharge  $Q_{rf}$  (red), the time series of simulated discharge (grey).

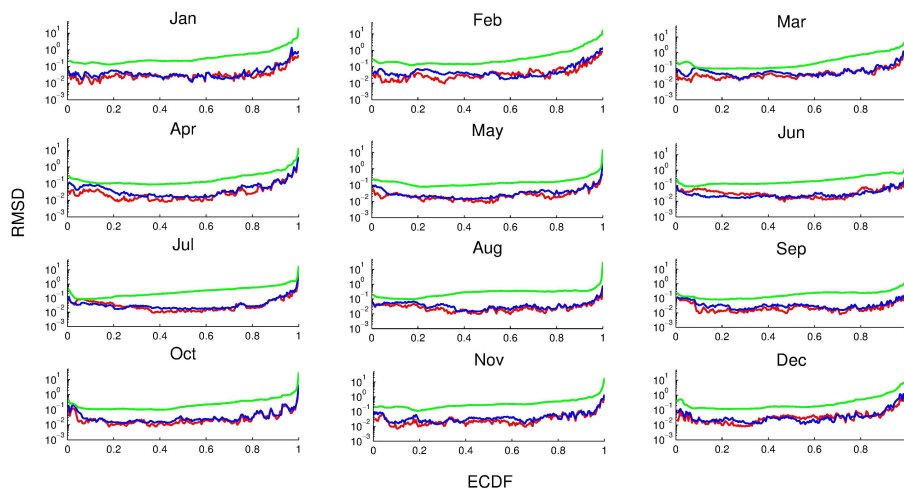


Figure 22: Root mean square difference (RMSD) for simulated discharge in different cases: case 1 (red), case 2 (blue) and case 3 (green).

424 In order to further investigate the quality of the simulated discharge for all cases, Fig. 21  
 425 presents the comparison between the ECDF of the daily averages of the modelled and reference  
 426 discharge for April, May and June. For all cases, the daily mean seems to be preserved by the  
 427 modelled discharge. However through investigating the width of the grey areas of the simulated  
 428 time series for each case, as expected, we can conclude that the most certain results are observed  
 429 in case 1, followed by case 2 and case 3. This also holds for the other months. Similar situations  
 430 are witnessed for the univariate return period of annual extreme discharge (Fig. 19) in which the  
 431 least and largest variations between the reference and simulated discharge are noticed for  $Q_{s1}$  and  
 432  $Q_{s3}$ , respectively. Especially, a remarkable expansion of grey areas is witnessed in case 3. It is  
 433 clear that each stochastic component, i.e. modelled precipitation, temperature or evapotranspiration,  
 434 has contributed an additional amount of variation to the modelled discharge. The differences  
 435 between the simulated discharge from different cases are less evident in terms of frequency distri-  
 436 butions but more pronounced for the mean and extreme discharge.

437  
 438 To account for the variations between the modelled and reference discharge, the simulated  
 439 discharge values are further evaluated using the root mean square deviation (RMSD):

$$\text{RMSD}(i) = \sqrt{\frac{1}{n} \sum_{s=1}^n (Q_{m,s}(i) - Q_o(i))^2} \quad (6)$$

440 where  $Q_m(i)$  and  $Q_o(i)$  are respectively the modelled and reference discharge value that have the  
 441 same value of cumulative frequency  $i \in [0, 1]$ ,  $i = 0.005, \dots, 1$  with a step of 0.005; and  $n$  is the  
 442 number of the members in the ensemble considered.

443  
 444 Figure 22 displays the RMSD calculated for simulated discharge in different cases. It can  
 445 be seen from the figure that for all cases, larger RMSD values are found for the higher values of  
 446 discharge. In other words, simulations of the higher values of discharge are generally less accurate.  
 447 There are insignificant differences between the RMSD for case 1 and 2 for all months. The use of  
 448 stochastically-generated temperature time series seemed to contribute minor uncertainty to the  
 449 discharge simulations in this study. The largest errors often are obtained in case 3 where the  
 450 discharge is simulated from stochastically-generated precipitation and evapotranspiration values.



## 451 5 Conclusions

452 In water management, discharge is a very important variable which can be simulated via a rainfall-  
 453 runoff model using recorded precipitation and evapotranspiration data. However, in situations that  
 454 suffer from data deficiency, one may consider using stochastically-generated time series. In this  
 455 study, the impact of using the stochastically-generated precipitation and evapotranspiration on  
 456 the simulation of the catchment discharge is investigated. In order to assess the influence of each  
 457 stochastic variable on the discharge simulations, three different cases have been considered. In  
 458 the first case, it is assumed that insufficient evapotranspiration data would be available, requir-  
 459 ing stochastically-generated evapotranspiration based on observed precipitation and temperature  
 460 data by means of a copula. In the second case, where only precipitation data would be sufficiently  
 461 available, the temperature and evapotranspiration are each reproduced by vine copulas. The third  
 462 case addresses the situation where too short time series of observations are available. In this case,  
 463 the precipitation time series could be generated using a Modified Bartlett-Lewis (MBL) model  
 464 calibrated to the limited precipitation data available and then the time series of temperature and  
 465 evapotranspiration could be obtained using the copula-based models. In all cases, the C-vine  
 466 copulas  $V_{TPE}$  and  $V_{T_pPT}$  are used for the simulations of evapotranspiration and temperature,  
 467 respectively. From the comparison between the simulations with the observations, the C-vine cop-  
 468 ulas seem to reproduce the time series of evapotranspiration and temperature well. It is clear that  
 469 each stochastic component has a certain impact on the discharge simulations, and each additional  
 470 stochastic variable will contribute an additional variation, and thus uncertainty. As expected,  
 471 the simulations of the discharge obtained for case 1 show the smallest variability, while those in  
 472 case 3 results in the largest variability. In general, no major differences are observed between the  
 473 simulations and observations in cases 1 and 2, the characteristics of the discharge series seem to be  
 474 preserved through the process for these cases. Noticeable variations are witnessed in case 3, where  
 475 the discharge is simulated using modeled time series of precipitation and evapotranspiration.

476 With respect to extreme discharge, it was shown that the uncertainties encountered in case 3  
 477 are highly reduced when using much longer time series as input than the maximum return period  
 478 aimed at. However, given that all forcing data are generated, the modeller is not restricted to  
 479 the length of an observed time series, but can generate time series of whatever length as input  
 480 to the hydrological model, taking into account that the longer the time series used, the more the  
 481 uncertainty reduces at the expense of increasing run-time.

482 From this study, we may thus conclude that in situations that suffer from a lack of observations,  
 483 one can rely on the stochastically-generated series of precipitation, temperature and evapotran-  
 484 spiration to reproduce time series of discharge for water resources management. However, care  
 485 should be taken as the modelled extreme discharges may experience the largest errors.

## 486 Acknowledgements

487 The authors gratefully acknowledge the Vietnamese Government Scholarship (VGS), the King  
 488 Baudouin Foundation (KBF) and the project G.0013.11N of the Research Foundation Flanders  
 489 (FWO) for their partial financial support for this work. The historical Uccle series were provided  
 490 by the Royal Meteorological Institute of Belgium.

## 491 References

- 492 Aas, K., Czado, C., Frigessi, A., and Bakken, H. (2009). Pair-copula constructions of multiple  
 493 dependence. *Insurance: Mathematics and Economics*, 44(2):182–198.
- 494 Abbott, M., Bathurst, J., Cunge, J., O’Connell, P., and Rasmussen, J. (1986). An introduction  
 495 to the European Hydrological System - Système Hydrologique Européen, SHE, 1: History and  
 496 philosophy of a physically-based, distributed modelling system. *Journal of Hydrology*, 87(1):45–  
 497 59.
- 498 Akaike, H. (1973). Information theory and an extension of the maximum likelihood principle. In  
 499 *Second International Symposium on Information Theory*, Budapest. Akadémiai Kiado.



- 500 Arnold, J. G., Srinivasan, R., Muttiah, R. S., and Williams, J. R. (1998). Large area hydrologic  
501 modeling and assessment. Part I: Model development. *Journal of the American Water Resources*  
502 *Association (JAWRA)*, 34(1):73–89.
- 503 Bedford, T. and Cooke, R. M. (2001). *Monte Carlo Simulation of Vine Dependent Random*  
504 *Variables for Applications in Uncertainty Analysis*. Management Science, theory, method and  
505 practice series. University of Strathclyde, Department of Management Science.
- 506 Bedford, T. and Cooke, R. M. (2002). Vines—a new graphical model for dependent random  
507 variables. *The Annals of Statistics*, 30(4):1031–1068.
- 508 Bergström, S. (1995). The HBV model. In: Singh, V.P. (Ed.) *Computer Models of Watershed*  
509 *Hydrology*. Water Resources Publications, Highlands Ranch, CO., pages 443–476.
- 510 Bernardara, P., De Michele, C., and Rosso, R. (2007). A simple model of rain in time: An  
511 alternating renewal process of wet and dry states with a fractional (non-Gaussian) rain intensity.  
512 *Atmospheric Research*, 84(4):291–301.
- 513 Boughton, W. and Droop, O. (2003). Continuous simulation for design flood estimation - a review.  
514 *Environmental Modelling and Software*, 18(4):309–318.
- 515 Cabus, P. (2008). River flow prediction through rainfall-runoff modelling with a probability –  
516 distributed model (PDM) in Flanders, Belgium. *Agricultural Water Management*, 95(7):859–  
517 868.
- 518 Cameron, D., Beven, K., and Tawn, J. (2000). An evaluation of three stochastic rainfall models.  
519 *Journal of Hydrology*, 228(1–2):130–149.
- 520 Cowpertwait, P. S. P., Isham, V., and Onof, C. (2007). Point process models of rainfall: develop-  
521 ments for fine-scale structure. *Proceedings of the Royal Society A: Mathematical, Physical and*  
522 *Engineering Science*, 463(2086):2569–2587.
- 523 Czado, C. (2010). Pair-copula constructions of multivariate copulas. In Jaworski, P., Durante,  
524 F., Härdle, W. K., and Rychlik, T., editors, *Copula Theory and Its Applications*, volume 198 of  
525 *Lecture Notes in Statistics*, pages 93–109. Springer Berlin Heidelberg.
- 526 Dai, Y., Zeng, X., Dickinson, R. E., Baker, I., Bonan, G. B., Bosilovich, M. G., Denning, A. S.,  
527 Dirmeyer, P. A., Houser, P. R., Niu, G., Oleson, K. W., Schlosser, C. A., and Yang, Z.-L. (2003).  
528 The Common Land Model. *Bulletin of the American Meteorological Society*, 84(8):1013–1023.
- 529 De Jongh, I. L. M., Verhoest, N. E. C., and De Troch, F. (2006). Analysis of a 105-year time series  
530 of precipitation observed at Uccle, Belgium. *International Journal of Climatology*, 26(14):2023–  
531 2039.
- 532 Démarée, G. R. (2003). Le pluviographe centenaire du plateau d’ Uccle: son histoire, ses données  
533 et ses applications. *Houille blanche*, 2003-004:95–102.
- 534 Droogers, P. and Allen, R. G. (2002). Estimating reference evapotranspiration under inaccurate  
535 data conditions. *Irrigation and Drainage Systems*, 16(1):33–45.
- 536 Gyasi-Agyei, Y. (1999). Identification of regional parameters of a stochastic model for rainfall  
537 disaggregation. *Journal of Hydrology*, 223(34):148–163.
- 538 Heneker, T. M., Lambert, M. F., and Kuczera, G. (2001). A point rainfall model for risk-based  
539 design. *Journal of Hydrology*, 247(1–2):54–71.
- 540 Kavvas, M. L. and Delleur, J. W. (1981). A stochastic cluster model of daily rainfall sequences.  
541 *Water Resources Research*, 17(4):1151–1160.
- 542 Kennedy, J. and Eberhart, R. (1995). Particle swarm optimization. In *Proceedings of the IEEE*  
543 *International Conference on neural networks*, pages 1942–1948.



- 544 Khaliq, M. N. and Cunnane, C. (1996). Modelling point rainfall occurrences with the modified  
545 Bartlett–Lewis rectangular pulses model. *Journal of Hydrology*, 180(1–4):109–138.
- 546 Kurowicka, D. and Cooke, R. M. (2007). Sampling algorithms for generating joint uniform distri-  
547 butions using the vine-copula method. *Computational Statistics and Data Analysis*, 51(6):2889–  
548 2906.
- 549 Mason, S. J. (2004). Simulating climate over Western North America using stochastic weather  
550 generators. *Climatic Change*, 62(1–3):155–187.
- 551 Moore, R. J. (2007). The PDM rainfall-runoff model. *Hydrology and Earth System Sciences*,  
552 11(1):483–499.
- 553 Nelsen, R. B. (2006). *An Introduction to Copulas*. Springer, New York.
- 554 Nielsen, S. A. and Hansen, E. (1973). Numerical simulation of the rainfall-runoff process on a  
555 daily basis. *Nordic Hydrol*, 3:171–190.
- 556 Ntegeka, V. and Willems, P. (2008). Trends and multidecadal oscillations in rainfall extremes,  
557 based on a more than 100-year time series of 10 min rainfall intensities at Uccle, Belgium. *Water*  
558 *Resources Research*, 44(7):W07402.
- 559 Onof, C., Chandler, R. E., Kakou, A., Northrop, P., Wheeler, H. S., and Isham, V. (2000). Rainfall  
560 modelling using Poisson-cluster processes: a review of developments. *Stochastic Environmental*  
561 *Research and Risk Assessment*, 14(6):384–411.
- 562 Onof, C. and Wheeler, H. S. (1993). Modelling of British rainfall using a random parameter  
563 Bartlett–Lewis rectangular pulse model. *Journal of Hydrology*, 149(1–4):67–95.
- 564 Onof, C., Wheeler, H. S., and Isham, V. (1994). Note on the analytical expression of the inter-  
565 event time characteristics for Bartlett–Lewis type rainfall models. *Journal of Hydrology*, 157(1–  
566 4):197–210.
- 567 Pham, M. T., Vanhaute, W. J., Vandenberghe, S., De Baets, B., and Verhoest, N. E. C. (2013).  
568 An assessment of the ability of Bartlett–Lewis type of rainfall models to reproduce drought  
569 statistics. *Hydrology and Earth System Sciences*, 17(12):5167–5183.
- 570 Pham, M. T., Vernieuwe, H., De Baets, B., Willems, P., and Verhoest, N. E. C. (2016). Stochas-  
571 tic simulation of precipitation-consistent daily reference evapotranspiration using vine copulas.  
572 *Stochastic Environmental Research and Risk Assessment*.
- 573 Rodriguez-Iturbe, I., Cox, D. R., and Isham, V. (1987a). Some models for rainfall based on  
574 stochastic point processes. *Proceedings of the Royal Society of London. Series A. Mathematical*  
575 *and Physical Sciences*, 410(1839):269–288.
- 576 Rodriguez-Iturbe, I., Cox, D. R., and Isham, V. (1988). A point process model for rainfall: Further  
577 developments. *Proceedings of the Royal Society of London. Series A. Mathematical and Physical*  
578 *Sciences*, 417(1853):283–298.
- 579 Rodriguez-Iturbe, I., De Power, B. F., and Valdes, J. B. (1987b). Rectangular pulses point process  
580 models for rainfall: Analysis of empirical data. *Journal of Geophysical Research*, 92(D8):9645–  
581 9656.
- 582 Salvadori, G. and De Michele, C. (2007). On the use of copulas in hydrology: Theory and practice.  
583 *Journal of Hydrologic Engineering*, 12(4):369–380.
- 584 Salvadori, G., De Michele, C., Kottegoda, N., and Rosso, R. (2007). *Extremes in Nature: An*  
585 *Approach Using Copulas*. Springer, New York.
- 586 Schepsmeier, U. (2015). Efficient information based goodness-of-fit tests for vine copula models  
587 with fixed margins: A comprehensive review. *Journal of Multivariate Analysis*, 138:34–52.





- 588 Sklar, A. (1959). Fonctions de répartition à  $n$  dimensions et leurs marges. *Publications de l'Institut*  
589 *de Statistique de l'Université de Paris*, (8):229–231.
- 590 Smithers, J. C., Pegram, G. G. S., and Schulze, R. E. (2002). Design rainfall estimation in South  
591 Africa using Bartlett–Lewis rectangular pulse rainfall models. *Journal of Hydrology*, 258(14):83–  
592 99.
- 593 Stern, R. D. and Coe, R. (1984). A model fitting analysis of daily rainfall data. *Journal of the*  
594 *Royal Statistical Society*, 147(1):1–34.
- 595 Todorovic, P. and Woolhiser, D. A. (1975). A stochastic model of  $n$ -day precipitation. *Journal of*  
596 *Applied Meteorology*, 14(1):17–24.
- 597 Vaes, G. and Berlamont, J. (2000). Selection of appropriate short rainfall series for design of  
598 combined sewer systems. In *Proceedings of 90 International Conference on Urban Drainage on*  
599 *Internet, Hydroinform, Czech Republic*.
- 600 Vandenberghe, S., Verhoest, N. E. C., Buyse, E., and De Baets, B. (2010). A stochastic design  
601 rainfall generator based on copulas and mass curves. *Hydrology and Earth System Sciences*,  
602 14(12):2429–2442.
- 603 Vanhaute, W., Vandenberghe, S., Scheerlinck, K., De Baets, B., and Verhoest, N. E. C. (2012).  
604 Calibration of the modified Bartlett–Lewis model using global optimization techniques and  
605 alternative objective functions. *Hydrology and Earth System Sciences*, 16(3):873–891.
- 606 Velghe, T., Troch, P. A., De Troch, F. P., and Van de Velde, J. (1994). Evaluation of cluster-based  
607 rectangular pulses point process models for rainfall. *Water Resources Research*, 30(10):2847–  
608 2857.
- 609 Verhoest, N. E. C., Troch, P., and De Troch, F. (1997). On the applicability of Bartlett–Lewis  
610 rectangular pulses models in the modeling of design storms at a point. *Journal of Hydrology*,  
611 202(14):108–120.
- 612 Verhoest, N. E. C., Vandenberghe, S., Cabus, P., Onof, C., Meca-Figueras, T., and Jameled-  
613 dine, S. (2010). Are stochastic point rainfall models able to preserve extreme flood statistics?  
614 *Hydrological Processes*, 24(23):3439–3445.
- 615 Viglione, A., Castellarin, A., Rogger, M., Merz, R., and Blöschl, G. (2012). Extreme rainstorms:  
616 Comparing regional envelope curves to stochastically generated events. *Water Resources Re-*  
617 *search*, 48(1):W01509.
- 618 Vrebos, D., Vansteenkiste, T., Staes, J., Willems, P., and Meire, P. (2014). Water displacement by  
619 sewer infrastructure in the Grote Nete catchment, Belgium, and its hydrological regime effects.  
620 *Hydrology and Earth System Sciences*, 18(3):1119–1136.
- 621 Wilks, D. S. (1998). Multisite generalization of a daily stochastic precipitation generation model.  
622 *Journal of Hydrology*, 210(1–4):178–191.
- 623 Wilks, D. S. and Wilby, R. L. (1999). The weather generation game: a review of stochastic weather  
624 models. *Progress in Physical Geography*, 23(3):329–357.
- 625 Willems, P. (2013). Adjustment of extreme rainfall statistics accounting for multidecadal climate  
626 oscillations. *Journal of Hydrology*, 490:126–133.
- 627 Woolhiser, D. A. and Roldán, J. (1982). Stochastic daily precipitation models: 2. A comparison  
628 of distributions of amounts. *Water Resources Research*, 18(5):1461–1468.